Available online at www.sciencedirect.com
SCIENCE DIRECT®
International Journal of Heat and Mass Transfer 47 (2004) 1413–1422
International Journal of HEAT and MASS TRANSFER
www.elsevier.com/locate/ijhmt

Natural convection from an elliptic tube with major axis horizontal and placed in a micropolar fluid

F.M. Mahfouz

Department of Mechanical Power, Faculty of Engineering, Menufiya University, Egypt

Received 24 February 2003

Abstract

In this paper the problem of natural convection from an isothermal elliptic tube with its major axis horizontal and placed in a micropolar fluid is investigated. The study is based on the solution of full conservation equations of mass, linear momentum, angular momentum and energy without boundary layer assumptions. The study focuses on the effect of the fluid material parameters and Rayleigh number on both flow and thermal fields. Prandtl number and ellipse axis ratio are kept constant. Results are presented for the local and average Nusselt numbers along with some details of both flow and thermal fields. In comparison with Newtonian fluids the study has shown that micropolar fluids display a reduction in heat transfer rate.

1. Introduction

Natural convection from cylindrical tubes to a surrounding fluid has many practical applications. These applications include nuclear reactors, heat exchangers, hot wires, cooling of electronic devices, steam pipes and many others. Previous studies have mainly focused on natural convection from surfaces with relatively simple geometry such as circular cylinders and flat plates and placed in Newtonian fluids. Morgan [1] has compiled the literature up to 1997 for the case of isothermal circular cylinders.

The interest in investigating natural convection from elliptic tubes placed in Newtonian fluids started when Lin and Chao [2] solved the boundary layer equations for the case of two dimensional and axisymmetric bodies with circular and elliptic cylinders as special cases. Raithby and Hollands [3] studied the natural convection from elliptic tube with its major axis vertical. They also considered different axis ratios with circular cylinder and flat plate as limiting cases. Their results for average Nusselt number were found to be in a good agreement with the experimental data. Merkin [4] solved the governing boundary layer equations for the case of natural convection from elliptic tube with major axis either horizontal or vertical. He presented results for local and averaged heat transfer rates for both constant surface temperature and constant surface heat flux. The analysis of natural convection from horizontal elliptic tubes placed in Newtonian fluids and based on the solution of full governing equations were carried out by Badr and Shamsher [5] and Badr [6]. Badr and Shamsher [5] considered the case of the tube major axis vertical while Badr [6] considered the case of tube at different orientations. Huang and Mayinger [7] studied experimentally the natural convection from elliptic tubes with different axis ratios and at different orientations. They reported results for the local and average Nusselt numbers together with a correlation for average Nusselt number.

Eringen [8] has proposed the theory of micropolar fluids. This theory takes into account the local effects arising from the microstructure and intrinsic motion of fluid elements. Such fluids can support surface and body couples which are not present in the theory of Newtonian fluids. Micropolar fluids are believed to be successful in describing the behavior of heterogeneous mixtures such as ferro liquids, colloidal fluids, animal blood, most slurries and some liquids with polymer additives. Eringen [9] developed the theory of thermo-micropolar fluids by extending his theory of micropolar fluids.

Previous studies of convective heat transfer in micropolar fluids have focused mainly on relatively simple geometry [10–16]. The only attempt made to investigate

0017-9310/$ - see front matter © 2003 Published by Elsevier Ltd.
doi:10.1016/j.ijheatmasstransfer.2003.09.025

Nomenclature

a	length of semi-major axis
Ar	axis ratio (b/a)
b	length of semi-minor axis
B	dimensionless spin viscosity
c'	ellipse eccentricity ($a\sqrt{1-Ar^2}$)
c	dimensionless ellipse eccentricity (c'/a)
f_n	Fourier coefficients
F_b	buoyancy force
$F_{x'}$, $F_{y'}$	components of buoyancy force in x', y' directions
g	gravitational acceleration
g_n	Fourier coefficients
Gr	Grashof number ($g\beta(2a)^3(T_s - T_\infty)/\nu^2$)
h, $\bar{h}$	local and average heat transfer coefficients
H_0, H_n	Fourier coefficients
k	thermal conductivity
K_v	vortex viscosity
j	microinertia density
M	dimensionless microrotation
Nu, $\overline{Nu}$	local and average Nusselt numbers
Pr	Prandtl number (ν/α)
Ra	Rayleigh number ($GrPr$)
t	dimensionless time
T	temperature
x', y'	Cartesian coordinates
x, y	dimensionless Cartesian coordinates
Y^*	the distance from the tube surface at along line $\eta = 90$, $\left(\frac{y'-a}{a}Ra^{0.25}\right)$

Greek symbols

α	thermal diffusivity
β	coefficient of thermal expansion
Δ	dimensionless vortex viscosity
ε	dimensionless length ($1/c$)
ϕ	dimensionless temperature $((T - T_\infty)/(T_s - T_\infty))$
η, ξ	elliptical coordinates
γ	spin gradient viscosity
μ	dynamic viscosity
λ	dimensionless spin gradient viscosity
ν	kinematics viscosity
ρ	density
σ	component of microrotation vector in x', y' plane
τ	time
ψ', ψ	dimensional and dimensionless stream functions
ζ', ζ	dimensional and dimensionless vorticity

Subscripts

s	at the tube surface
∞	at infinite distance from the tube surface

the case of natural convection from an elliptic cylinder placed in a micropolar fluid was carried out by Bhattacharyya and Pop [17]. In their study steady natural convection from isothermal elliptic tube with its major axis either horizontal or vertical was considered. They solved the boundary layer equations using a solution procedure similar to that of Merkin [4]. They presented results for local Nusselt number along with velocity and temperature fields.

The main objective of this study is to analyze the natural convection from an isothermal horizontal elliptic tube placed in a micropolar fluid. The analysis is based on the solution of full governing equations using spectral Fourier series expansion method. The local and average Nusselt numbers are presented as well as some details of both flow and thermal fields. The buoyancy driven flow is assumed laminar and two dimensional.

2. Problem formulation

Fig. 1 shows the physical model and coordinates system, consisting of an isothermal horizontal elliptic tube of infinite length placed with its major axis horizontal in a quiescent micropolar fluid at temperature T_∞. The buoyancy driven flow is assumed to be laminar and two-dimensional. The effect of viscous dissipation and micropolar heat conduction is assumed to be negligible and the fluid properties are assumed to be constant. The conservation equations of mass, linear momentum, angular momentum and energy for a micropolar fluid are

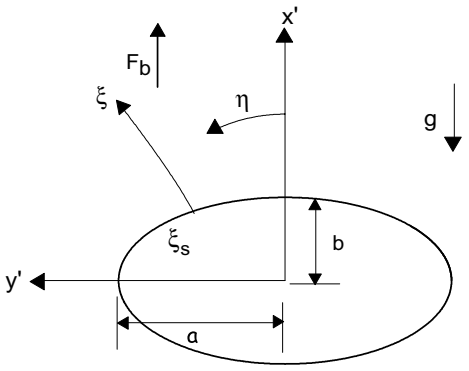

Fig. 1. Physical model and coordinate system.

based on the model developed by Eringen [8,9]. These equations within Boussinesq approximation can be written in terms of vorticity, stream function, microrotation and temperature as:

$$\frac{\partial\zeta'}{\partial\tau}+\frac{\partial\psi}{\partial y'}\frac{\partial\zeta'}{\partial x'}-\frac{\partial\psi}{\partial x'}\frac{\partial\zeta'}{\partial y'}=\left(v+\frac{K_v}{\rho}\right)\nabla^2\zeta'-\frac{K_v}{\rho}\nabla^2\sigma+\frac{1}{\rho}\left[\frac{\partial F_{y'}}{\partial x'}-\frac{\partial F_{x'}}{\partial y'}\right] \quad (1)$$

$$\zeta'=-\nabla^2\psi' \quad (2)$$

$$\frac{\partial\sigma}{\partial\tau}+\frac{\partial\psi'}{\partial y'}\frac{\partial\sigma}{\partial x'}-\frac{\partial\psi'}{\partial x'}\frac{\partial\sigma}{\partial y'}=\frac{\gamma}{\rho j}\nabla^2\sigma+\frac{K_v}{\rho j}(\zeta'-2\sigma) \quad (3)$$

$$\frac{\partial T}{\partial\tau}+\frac{\partial\psi'}{\partial y'}\frac{\partial T}{\partial x'}-\frac{\partial\psi'}{\partial x'}\frac{\partial T}{\partial y'}=\frac{k}{\rho c_v}\nabla^2 T \quad (4)$$

where

$$\nabla^2=\frac{\partial^2}{\partial x'^2}+\frac{\partial^2}{\partial y'^2}$$

τ is the time, ρ is the density, v is the kinematic viscosity, k is the thermal conductivity and c_v is the specific heat. K_v, j and γ are the vortex viscosity, microinertia density and spin-gradient viscosity. ζ' is the vorticity, ψ' is the stream function, T is the temperature and σ is the component of microrotation vector whose direction of rotation is in the $x'-y'$ plane. $F_{x'}=\rho g\beta(T-T_\infty)$, $F_{y'}=0$ are the components of the buoyancy force, where β is the coefficient of thermal expansion of the fluid.

The boundary conditions are mainly the no-slip and impermeability conditions on the tube surface and the stagnant ambient conditions very far away from it. These boundary conditions can be expressed as:

$$\psi'=\frac{\partial\psi'}{\partial x'}=0,\quad \frac{\partial\psi'}{\partial y'}=0,\quad T=T_s \quad \text{and}$$
$$\sigma=0 \quad \text{on the tube surface} \quad (5a)$$

$$\frac{\partial\psi'}{\partial x'}\to 0,\quad \frac{\partial\psi'}{\partial y'}\to 0,\quad T\to T_\infty \quad \text{and}$$
$$\sigma\to 0 \quad \text{far away from the tube surface} \quad (5b)$$

The following dimensionless variables are now introduced:

$$x=\frac{x'}{a},\quad y=\frac{y'}{a},\quad t=\frac{\tau\alpha}{a^2},\quad \psi=\frac{\psi'}{\alpha},\quad \zeta=-\zeta'\frac{a^2}{\alpha},$$
$$M=\frac{a^2\sigma}{\alpha},\quad \Delta=\frac{\rho K_v}{v},\quad B=\frac{a^2}{j},\quad \lambda=\frac{\rho\gamma}{jv} \quad \text{and}$$
$$\phi=\frac{T-T_\infty}{T_s-T_\infty}$$

where a is the length of semi-major axis and α is the thermal diffusivity of the fluid.

To prepare Eqs. (1)–(4) for accurate numerical treatment it is more appropriate to use elliptic coordinates ξ, η defined as

$$\xi+i\eta=\varepsilon\sinh^{-1}(x+iy)$$

where $\varepsilon=1/c$, c is the dimensionless ellipse eccentricity. Using the above transformation, the dimensionless form of Eqs. (1)–(4) in the elliptic coordinates read the following:

$$J\frac{\partial\zeta}{\partial t}=Pr(1+\Delta)\left(\frac{\partial^2\zeta}{\partial\xi^2}+\frac{\partial^2\zeta}{\partial\eta^2}\right)+\frac{\partial\psi}{\partial\xi}\frac{\partial\zeta}{\partial\eta}-\frac{\partial\psi}{\partial\eta}\frac{\partial\zeta}{\partial\xi}+Pr\Delta\left(\frac{\partial^2 M}{\partial\xi^2}+\frac{\partial^2 M}{\partial\eta^2}\right)+\frac{RaPr}{8\varepsilon}\left[\sinh\xi\sin\eta\frac{\partial\phi}{\partial\xi}+\cosh\xi\cos\eta\frac{\partial\phi}{\partial\eta}\right] \quad (6)$$

$$J\zeta=\frac{\partial^2\psi}{\partial\xi^2}+\frac{\partial^2\psi}{\partial\eta^2} \quad (7)$$

$$J\frac{\partial M}{\partial t}=\frac{\partial\psi}{\partial\xi}\frac{\partial M}{\partial\eta}-\frac{\partial\psi}{\partial\eta}\frac{\partial M}{\partial\eta}+Pr\lambda\left(\frac{\partial^2 M}{\partial\xi^2}+\frac{\partial^2 M}{\partial\eta^2}\right)-J\Delta BPr(\zeta+2M) \quad (8)$$

$$J\frac{\partial\phi}{\partial t}=\left(\frac{\partial^2\phi}{\partial\xi^2}+\frac{\partial^2\phi}{\partial\eta^2}\right)+\frac{\partial\psi}{\partial\xi}\frac{\partial\phi}{\partial\eta}-\frac{\partial\psi}{\partial\eta}\frac{\partial\phi}{\partial\xi} \quad (9)$$

where $J=(\cosh^2\xi-\sin^2\eta)/\varepsilon^2$, $Ra=GrPr$ is the Rayleigh number, $Gr=g\beta(2a)^3(T_s-T_\infty)/v^2$ is the Grashof number and $Pr=v/\alpha$ is the Prandtl number.

The boundary conditions (5) can now be expressed as

$$\psi=\frac{\partial\psi}{\partial\xi}=0,\quad \frac{\partial\psi}{\partial\eta}=0,\quad M=0 \quad \text{and}$$
$$\phi=1 \quad \text{at } \xi=\xi_s \quad (10a)$$

$$\frac{\partial\psi}{\partial\xi}\to 0,\quad \frac{\partial\psi}{\partial\eta}\to 0,\quad M\to 0 \quad \text{and}$$
$$\phi\to 0 \quad \text{as } \xi\to\infty \quad (10b)$$

where ξ_s defines the ellipse surface ($=\tanh^{-1}b/a$).

The temperature of the stagnant fluid around the tube at times $t<0$ is T_∞ ($\phi=0$) which is the same as that of the tube surface. At the start of computations ($t=0$) the tube surface assumes a sudden temperature increase from T_∞ to T_s ($\phi=1$), and from that moment the time development of both flow and thermal fields starts.

3. The method of solution

The method used for solving the governing equations (6)–(9) to obtain the time development of both velocity and temperature fields is based on approximating the stream function, vorticity, microrotation and

temperature using Fourier series expansion. The approach is similar to that used by Collins and Dennis [18] and by Badr and Dennis [19]. The stream function ψ, vorticity ζ, microrotation M and temperature ϕ are now approximated as

$$\psi = \sum_{n=1}^{N} f_n \sin(n\eta) \quad n = 1, 2, N \tag{11a}$$

$$\zeta = \sum_{n=1}^{N} g_n \sin(n\eta) \tag{11b}$$

$$M = \sum_{n=1}^{N} r_n \sin(n\eta) \tag{11c}$$

$$\phi = H_0 + \sum_{n=1}^{N} H_n \cos(n\eta) \tag{11d}$$

where N is the number of terms in the Fourier series. The functions f_n, g_n, r_n, H_0 and H_n are Fourier coefficients and all are dependent on ξ and t. Substitution of Eqs. (11a)–(11d) in Eqs. (6)–(9) results in the following set of differential equations:

$$\frac{\partial^2 f_n}{\partial \xi^2} - n^2 f_n = \frac{1}{2\varepsilon^2}\left(\cosh 2\xi g_n + \frac{1}{2}\left[g_{(n+2)} + \operatorname{sgn}(n-2) g_{|n-2|}\right]\right) \tag{12}$$

$$\cosh 2\xi \frac{\partial g_n}{\partial t} + \frac{1}{2}\left[\frac{\partial g_{(n+2)}}{\partial t} + \operatorname{sgn}(n-2)\frac{\partial g_{|n-2|}}{\partial t}\right] = 2\varepsilon^2 Pr(1+\Delta)\left(\frac{\partial^2 g_n}{\partial \xi^2} - n^2 g_n\right) + S_n \tag{13}$$

$$\cosh 2\xi \frac{\partial r_n}{\partial t} + \frac{1}{2}\left[\frac{\partial r_{(n+2)}}{\partial t} + \operatorname{sgn}(n-2)\frac{\partial r_{|n-2|}}{\partial t}\right] = 2\varepsilon^2 Pr\lambda\left(\frac{\partial^2 r_n}{\partial \xi^2} - n^2 r_n\right) + K_n \tag{14}$$

$$\cosh 2\xi \frac{\partial}{\partial t}\begin{pmatrix} H_0 \\ H_n \end{pmatrix} + \frac{1}{2}\frac{\partial}{\partial t}\begin{bmatrix} H_2 \\ H_{(n+2)} \end{bmatrix} + \frac{1}{2}\frac{\partial}{\partial t}\begin{bmatrix} 0 \\ H_{|n+2|} \end{bmatrix} = 2\varepsilon^2 \frac{\partial^2}{\partial \xi^2}\begin{pmatrix} H_0 \\ H_n \end{pmatrix} - 2n^2\varepsilon^2 \begin{pmatrix} 0 \\ H_n \end{pmatrix} + \begin{pmatrix} Z_0 \\ Z_n \end{pmatrix} \tag{15}$$

where $\operatorname{sgn}(n-2)$ means the sign of term $(n-2)$ and $\operatorname{sgn}(n-2) = g_{|n-2|} = r_{|n-2|} = 0$, $H_{|n-2|} = H_0$ for $n = 2$. The terms S_n, K_n, Z_0 and Z_n are all easily identifiable functions of ξ and t.

The boundary conditions for all functions presented in equations (12)–(15) are obtained from Eqs. (10) and can be expressed as

$$f_n = r_n = H_n = 0, \quad H_0 = 2, \quad \frac{\partial f_n}{\partial \xi} = 0 \quad \text{at } \xi = \xi_s \quad \text{and} \quad \frac{1}{J^{1/2}} f_n, \frac{1}{J^{1/2}}\frac{\partial f_n}{\partial \xi}, \quad g_n,\ r_n,\ H_0,\ H_n \to 0 \quad \text{as } \xi \to \infty \tag{16}$$

Integrating the both sides of Eq. (12) with respect to ξ (after multiplying by $e^{-n\xi}$) from $\xi = \xi_s$ to $\xi = \infty$ and using the boundary conditions (16) one obtains the integral condition:

$$\int_{\xi_s}^{\infty} e^{-n\xi}\left(\cosh 2\xi g_n + \frac{1}{2}\left[g_{(n+2)} + \operatorname{sgn}(n-2) g_{|n-2|}\right]\right) d\xi = 0. \tag{17}$$

The above integral condition is used to get the values of the function g_n on the tube surface which is then substituted in Eq. (11b) to get the surface vorticity distribution.

The initial values ($t = 0$) for Fourier coefficients can be written as

$$f_n(\xi, 0) = g_n(\xi, 0) = r_n(\xi, 0) = H_n(\xi, 0) = 0, \quad \text{for } 1 \leqslant n \leqslant N, \xi \geqslant \xi_s$$
$$H_0(\xi, 0) = 2 \quad \text{for } \xi = \xi_s \quad \text{and} \quad H_0(\xi, 0) = 0 \quad \text{for } \xi > \xi_s \tag{18}$$

The number of points used in the ξ direction is 200 with a grid size taken as 0.05. This approximates the outer boundary at infinity at $\xi_{max} = \xi_s + 10$, which corresponds to a very large distance from the tube surface. Such large distance is necessary to ensure that the conditions at infinity are appropriately incorporated in the numerical solution. The logarithmic nature of the ξ coordinate enables us to have equal space steps in the numerical treatment while the physical space steps are gradually growing from very small space steps near the surface to large ones far away. This matches quite well the physical situation where steep variations near the surface exist. The number of terms in Fourier series is taken as five terms at the start and then more terms are added as the time elapses until reaching the steady state. The maximum number of terms N used in most of the cases considered was 40. The solution procedure is the same as that described by Badr and Dennis [19] and Mahfouz and Badr [20]. The only difference is the appearing of the unknown terms $g_{(n+2)}$, $r_{(n+2)}$ and $H_{(n+2)}$ in Eqs. (12)–(15). These terms were first approximated and corrected through an iterative procedure every time step.

The local and average Nusselt numbers are defined as

$$Nu = 2ah/k, \quad \overline{Nu} = 2a\bar{h}/k \tag{19}$$

where k is the fluid thermal conductivity and h and $\bar{h}$ are the local and averaged heat transfer coefficients. The local heat transfer coefficient is defined as

$$h = \dot{q}/(T_s - T_\infty), \quad \dot{q} = -k(\partial T/\partial S_n)_{\xi_s} \tag{20}$$

where, $\dot{q}$ is the rate of heat transfer per unit area, S_n is the normal direction to ellipse surface. From the above

definitions one can deduce the relation between the Nu and Fourier coefficients H_0 and H_n

$$Nu = -2\left(J^{-1/2}\frac{\partial\phi}{\partial\xi}\right)_{\xi_s} = -J_s^{-1/2}\left[\frac{\partial H_0}{\partial\xi} + 2\sum_{n=1}^{n=N}\frac{\partial H_n}{\partial\xi}\cos n\eta\right]_{\xi_s} \quad (21)$$

where $J_s = (\cosh^2\xi_s - \sin^2\eta)/\varepsilon^2$.

The averaged heat transfer coefficient is defined as $\bar{h} = \frac{1}{P}\int_0^P h\,dP$ where P is the perimeter of the elliptic section. The averaged Nusselt number can now be expressed as

$$\overline{Nu} = \frac{1}{P}\int_0^P Nu\,dP = -\frac{2\pi a}{P}\left(\frac{\partial H_0}{\partial\xi}\right)_{\xi=\xi_s} \quad (22)$$

4. Results and discussion

The governing equations along with the boundary conditions were solved in order to get the details of both flow and thermal fields. The main controlling parameters are Rayleigh number Ra, Prandtl number Pr, axis ratio Ar and the material parameters Δ, B and λ. For the sake of brevity only the effect of Ra, Δ and B are considered while Pr, λ and Ar are kept unchanged. The Ra number is considered in its moderate range up to 10^4. The study considered dimensionless vortex viscosity parameter Δ in the range from 0 to 5 and dimensionless microinertia density, B in the range from 0.1 to 10. The spin gradient viscosity parameter λ is fixed at value of 1. These values for material parameters are chosen to satisfy the thermodynamics restrictions given by Eringen [9]. The Prandtl number is kept constant at 0.7 while the axis ratio Ar is kept at 0.6. In this study, however, different values for these controlling parameters are chosen whenever comparisons with previous results are considered.

The accuracy of the method of solution is first verified by comparing the present results with the most relevant results in the literature. Fig. 2 shows a comparison between the present result for the steady-state Nu with the numerical results of Badr [5] for the case of natural convection from elliptic tube with major axis horizontal at $Ra = 10^4$, $Ar = 0.4$ and placed in Newtonian fluid ($\Delta = 0$). Shown in the same figure are the experimental results (modified to match present definition for Nu) of Haung and Mayinger [7] for $Ar = 0.389$. The figure shows very good agreement with that of Badr [6] and good agreement with that of Haung and Mayinger [7]. The steady state local Nusselt number distribution at $Ra = 10^5$ for the special limiting case of circular cylinder ($Ar = 0.998$) and placed in Newtonian

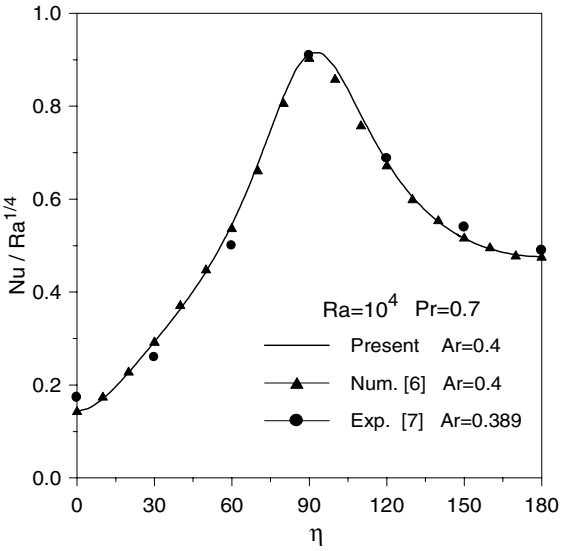

Fig. 2. Local Nusselt number distribution for the case of $Ra = 10^4$, $Ar = 0.4$, $Pr = 0.7$ and comparison with numerical results of [6] and experimental results of [7].

fluid is shown in Fig. 3 together with the numerical and experimental results reported by Kuehn and Goldstein [21]. The numerical results of Saitoh et al. [22] for the same case are shown also in the same figure. The figure shows satisfactory agreement especially with the bench mark solution of Saitoh et al. [22].

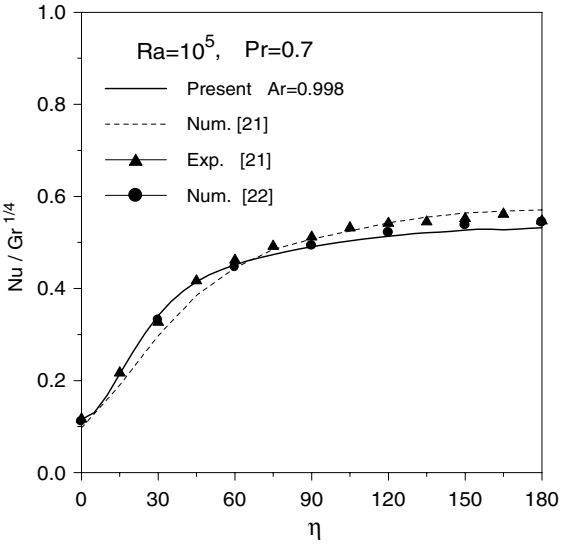

Fig. 3. Local Nusselt number distribution for the case of circular cylinder at $Ra = 10^5$ and a comparison with results of [21,22].

Table 1 shows the effect of Ra number and the material parameters Δ and B of a micropolar fluid on the steady state average Nusselt number, $\overline{Nu}$. It can be seen that the effect of Ra on steady-state $\overline{Nu}$ is quite clear, that is at any fixed value of fluid material parameters as Ra increases the $\overline{Nu}$ increases. This is quite expected since increasing of Ra leads to increasing of convection currents intensity and so increasing the heat transfer rate. Also, it can be seen that as the material parameter Δ increases at any fixed value of Ra the $\overline{Nu}$ decreases. The table also shows that the effect of parameter B on steady $\overline{Nu}$ in the range considered for parameters is almost negligible.

Fig. 4 shows the time variation of average Nusselt number $\overline{Nu}$ for the case of Rayliegh number, $Ra = 10^4$, $Ar = 0.6$ and at different values of dimensionless vortex viscosity $\Delta = 0, 1, 2, 5$. The figure clearly shows that the general variation of average Nusselt number is similar to that for Newtonian fluid ($\Delta = 0$). That is immediately after the tube temperature is increased the conduction mode of heat transfer is prevailing with high values of $\overline{Nu}$ due to high temperature gradient near the tube surface. In this early time stages a quick decrease in heat transfer rate occurs, reaching to a minimum value at a certain time. Beyond this time, the buoyancy force starts dominating, causing the fluid to set in motion and hence transition to the convection mode. The transition from conduction mode domination to convection mode domination takes the form of overshoot in heat transfer. At later times the convection dominated heat transfer rate gradually approaches its steady state value.

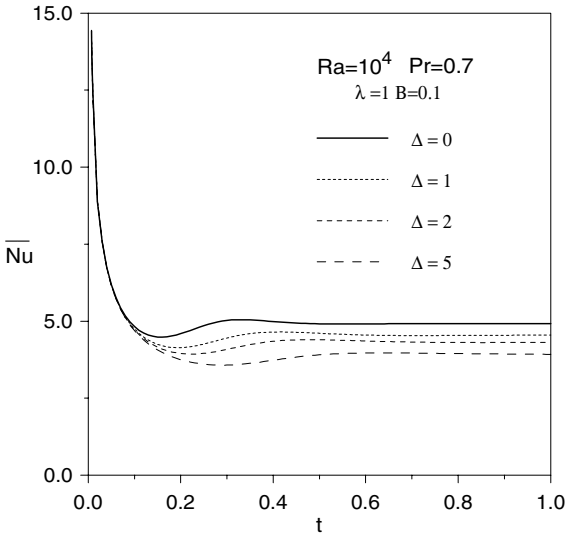

Fig. 4. The time variation of average Nusselt number for the case of $Ra = 10^4$, $Pr = 0.7$ $Ar = 0.6$, $\lambda = 1$, $B = 0.1$ and at different values of Δ.

Table 1
Effect of Rayleigh number and material parameters and B on steady state average Nusselt number

Ar	Ra	Δ	B	$\overline{NU}$
0.6	100	–	–	2.105
		1	0.1	1.998
		2	0.1	1.931
		5	0.1	1.792
		1	1	2.030
		2	1	1.935
		5	1	1.751
		1	10	2.045
		2	10	1.972
		5	10	1.809
	1000	–	–	3.143
		1	0.1	2.931
		2	0.1	2.814
		5	0.1	2.604
		1	1	2.926
		2	1	2.806
		5	1	2.611
		1	10	2.932
		2	10	2.830
		5	10	2.678
	10 000	–	–	4.921
		1	0.1	4.544
		2	0.1	4.309
		5	0.1	3.922
		1	1	4.543
		2	1	4.310
		5	1	3.919
		1	10	4.544
		2	10	4.329
		5	10	3.990

–, Refers to Newtonian fluid.

It can be observed from the figure that the average steady heat transfer rates in the case of micropolar fluids ($\Delta = 1, 2, 5$) is lower than that for Newtonian fluid ($\Delta = 0$). This decrease was attributed to the increase of the effect of vortex viscosity which makes the fluid flow more viscous and so weakens the convection currents. In the initial stages where the conduction mode of heat transfer is dominant there is no effect for vortex viscosity and the heat transfer rates for micropolar fluid and Newtonian fluid are identical. As the convection mode starts dominating the vortex viscosity of micropolar fluid enhances the flow viscosity and so weakens the convection currents which in turn decreases the heat transfer rate. The larger the value of vortex viscosity Δ the larger the flow viscosity and the lower the value of steady state $\overline{Nu}$. Decreasing of heat transfer rates as the vortex viscosity Δ increases is reported in the works of Mahfouz [15] and Hsu et al. [16].

Fig. 5 shows the steady local Nusselt number distribution over the elliptic tube surface for the case of $Ar = 0.75$, $\Delta = 1.5$, $\lambda = 0.5$ and $Pr = 1$ and at different

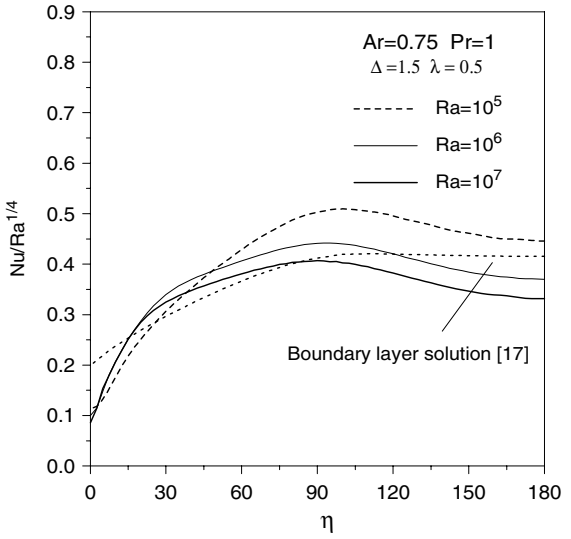

Fig. 5. Local Nusselt number distribution for the case of $Ar = 0.75$, $Pr = 1$, $\lambda = 0.5$, $\Delta = 1.5$ at different Ra and comparison with boundary layer solution [17].

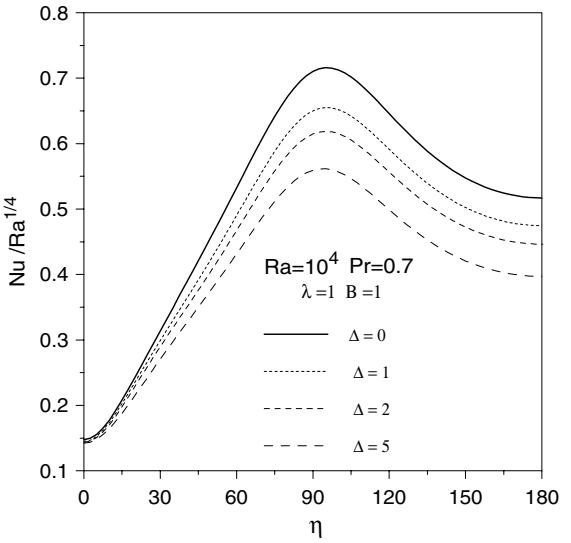

Fig. 6. Local steady state Nusselt number distribution for the case of $Ra = 10^4$, $Pr = 0.7$ $Ar = 0.6$, $\lambda = 1$, $B = 0.1$ and at different values of Δ.

Rayleigh numbers. The values of Rayleigh number are higher than the range considered for focusing the study. This is to be able to compare results with the boundary layer solution obtained by Bhattacharyya and Pop [17]. The boundary layer result shown in the same figure may be the limiting case as $Ra \to \infty$ for laminar flow excluding the plume region. At $Ra = 10^7$ the deviation of the local heat transfer based on boundary layer solution from that obtained from present calculation is small in the range $20 \leqslant \eta \leqslant 110$ with maximum difference of about 8% at $\eta = 31$. However, this difference increases over the remaining part of the ellipse surface, (i.e $0 < \eta < 20$ and $110 < \eta < 180$) reaching about 25% in the front stagnation region at $\eta = 180$ and about 130% in the rear stagnation region at $\eta = 0$. It is believed, unlike the case of circular cylinder or even the case of elliptic tube with major axis vertical, the boundary layer assumptions for elliptic tube with major axis horizontal are not only inappropriate in the plume region but also in the front stagnation region. In these two regions thick thermal and momentum boundary layers are formed due to surface geometry and inaccurate results are expected if the streamwise momentum and thermal diffusion are neglected.

The steady-state local Nusselt number distributions at $Ra = 10^4$, $Ar = 0.6$ and at different values of dimensionless vortex viscosity is shown in Fig. 6. Since the thermal field is symmetrical about the vertical axis, only one half of Nu distribution is shown. It can be seen at the topmost point on the tube surface ($\eta = 0$) the Nu is minimum and almost the same for all values of Δ. As η increases from topmost point ($\eta = 0$) to bottommost point ($\eta = 180$), the Nu increases for all values of Δ, reaching a maximum at almost $\eta = 95$ and then gradually decreases up to $\eta = 180$. Decreasing of Nu distributions at all points on the tube surface as Δ increases explains the decrease of steady state $\overline{Nu}$ as Δ increases as shown in Table 1. and Fig. 4.

Fig. 7 shows the surface vorticity distribution for the same case. It can be seen that the maximum absolute

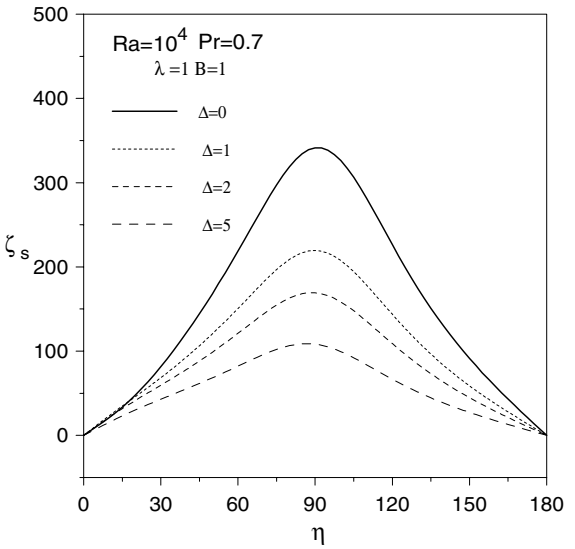

Fig. 7. Steady-state surface vorticity distribution for the case of $Ra = 10^4$, $Pr = 0.7$ $Ar = 0.6$, $\lambda = 1$, $B = 0.1$ and at different values of Δ.

surface vorticity occurs almost at $\eta = 90$, the point at which *Nu* assumes its maximum value. This link between surface vorticity and local heat transfer rate is different from that for the cases of circular cylinder and elliptic tubes with major axis vertical (see [5]). In these two latter cases the surface vorticity is zero at the front stagnation point where the *Nu* is maximum. The figure also shows that as Δ increases the surface vorticity decreases at all surface points. Decreasing of surface vorticity means decreasing of velocity gradients at the surface of the tube which means a weakness in convection currents and so a decrease in heat transfer rate.

Fig. 8 shows the steady state temperature distribution along the extension of ellipse major axis ($\eta = 90$) for the case of $Ra = 10^3$ and at different values of dimensionless vortex viscosity, Δ. The figure shows that the temperature decreases with distances until it reaches the ambient temperature at Y^* almost equal to value of 7. The figure clearly shows that as Δ increases the temperature gradient at the tube surface decreases which explains the decrease of heat transfer rate.

Figs. 9 and 10 show both steady flow field, in terms of streamlines, and steady thermal field, in terms of isotherms, as well as steady vorticity and microrotation fields for the case of $\lambda = 1$, $\Delta = 5$, $B = 1$ and at three Rayleigh numbers, $Ra = 100$, 1000 and 10000. Since these fields are symmetrical about the vertical axis, only one half of each field is considered. Fig. 9 shows the streamlines and isotherms patterns while Fig. 10 shows the equi-vorticity and equi-microrotation patterns. Fig. 9 clearly shows that as Rayleigh number increases both

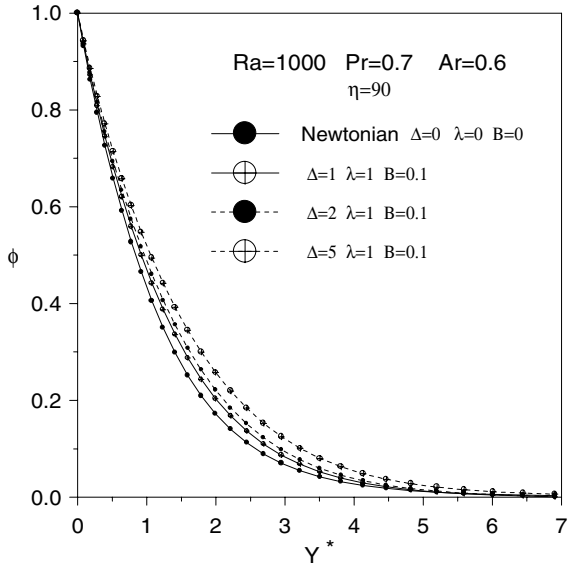

Fig. 8. Dimensionless temperature distribution along line ($\eta = 90$) for the case of $Ra = 10^3$, $Pr = 0.7$, $Ar = 0.6$, $\lambda = 1$, $B = 0.1$ and at different values of Δ.

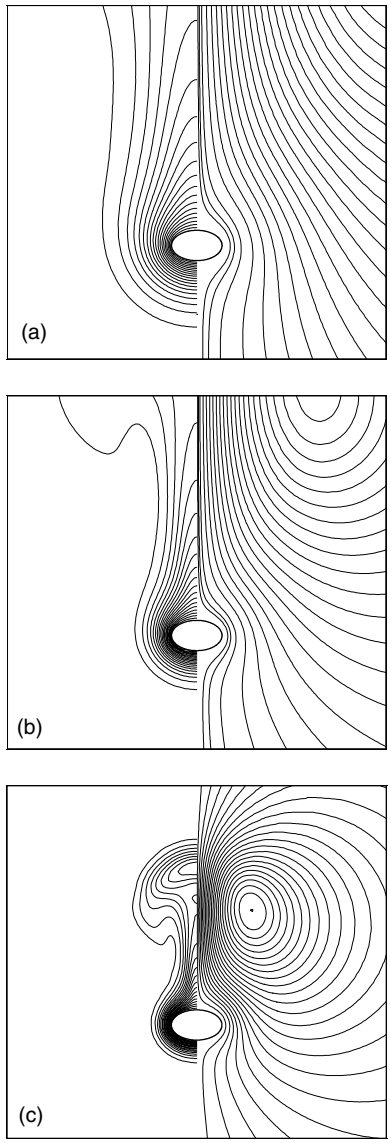

Fig. 9. The steady streamlines (right) and isotherms patterns (left) for the case of $Ar = 0.6$, $Pr = 0.7$, $\lambda = 1$, $\Delta = 5$ and $B = 1$: (a) $Ra = 10^2$ (b) $Ra = 10^3$ and (c) $Ra = 10^4$.

streamlines and isotherms are getting closer to the tube surface, indicating thinner momentum and thermal boundary layers. The same effect can be observed in Fig. 10, where zero vorticity line and zero angular velocity line (dashed lines in both sides) are getting closer to the surface as *Ra* increases. Fig. 10 also shows that both vorticity and microrotation fields are very similar with zero vorticity and microrotation lines are almost similar with a little deviation at the top of the tube (i. e. $\eta = 0$). This deviation between vorticity (regional rotation) and microrotation (elements microrotation) can be attributed to the inertia of fluid elements microrotation.

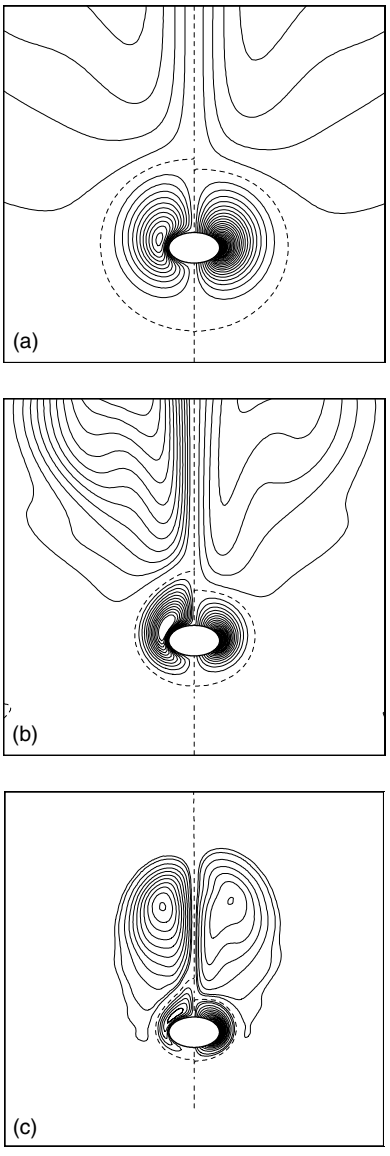

Fig. 10. The steady equi-vorticity (right) and microrotation (left) patterns for the case of $Ar = 0.6$, $Pr = 0.7$, $\lambda = 1$, $\Delta = 5$ and $B = 1$: (a) $Ra = 10^2$; (b) $Ra = 10^3$ and (c) $Ra = 10^4$.

5. Conclusions

The effect of material parameters of micropolar fluid and Rayleigh number on natural heat convection from an isothermal elliptic tube with major axis horizontal and placed in a micropolar fluid is investigated. The full governing equations of linear momentum, angular momentum and energy have been solved to give the details of flow and thermal fields. In this study the dimensionless spin gradient viscosity, λ Prandtl number, Pr and axis ratio, Ar are kept unchanged at 1, 0.7 and 0.6, respectively, while the study considered a range for Ra up to 10^4, a range for dimensionless vortex viscosity, Δ from 0 to 5 and a range for spin viscosity, B from 0.1 to 10. The study showed that at certain values for material parameters as Rayleigh number increases the local heat transfer rate increases at all points on the cylinder surface which in turn increases the average heat transfer rate. The study has also shown that the vortex viscosity is the most important material parameter. A noticeable reduction in local and average heat transfer rates is observed as vortex viscosity increases. Generally, the study showed that the convective heat transfer rate decreases in the micropolar fluids in comparison with the Newtonian fluids.

References

[1] V.T. Morgan, Heat transfer by natural convection from a horizontal isothermal circular cylinder in air, Heat Transfer Eng. 18 (1) (1997) 25–33.
[2] F.N. Lin, B.T. Chao, Laminar free convection over two dimensional and axisymmetric bodies of arbitrary contour, ASME J. Heat Transfer 96 (1974) 435–442.
[3] G.D. Raithby, K.G.T. Hollands, Laminar and turbulent free convection from elliptic cylinders with a vertical plate and horizontal circular cylinder as special cases, ASME J. Heat Transfer 98 (1976) 72–80.
[4] J.H. Merkin, Free convection boundary layers on cylinders of elliptic cross section, ASME J. Heat Transfer 99 (1977) 453–457.
[5] H.M. Badr, K. Shamsher, Free convection from an elliptic cylinder with major axis vertical, Int. J. Heat Mass Transfer 36 (14) (1993) 3593–3602.
[6] H.M. Badr, Laminar natural convection from an elliptic tube with different orientations, ASME J. of Heat Transfer 119 (1997) 709–718.
[7] S.Y. Huang, F. Mayinger, Heat transfer with natural convection around elliptic tubes, Wärm. Stoffübertrag. 18 (1984) 175–183.
[8] A.C. Eringen, Simple micropolars, Int. J. Eng. Sci. 2 (1964) 205–217.
[9] A.C. Eringen, Theory of thermomicrofluids, J. Math. Anal. Appl. 38 (1972) 480–496.
[10] A.A. Mohammadein, R.S.R. Gorla, Heat transfer in a micropolar fluid over a stretching sheet with viscous dissipation and internal heat generation, Int. J. Numer. Methods Heat Fluid Flow 11 (1) (2001) 50–58.
[11] I.A. Hassanien, Mixed convection in micropolar boundary layer flow over a horizontal semi-infinite plate, ASME, J. Fluids Eng. 118 (1996) 833–838.
[12] G. Ahmadi, Self-Similar solution of incompressible micropolar boundary layer flow over a semi-infinite plate, Int. J. Eng. Sci. 14 (1976) 639–646.
[13] R.S.R. Gorla, Axisymmetric thermal boundary layer of a micropolar fluid on a cylinder, Int. J. Eng. Sci. 23 (1995) 401–407.
[14] A.A. Mohammedien, R.S.R. Gorla, I.A. Hassanien, Mixed convection in an axisymmetric stagnation flow of

micropolar fluid on a vertical cylinder, Acta Mech. 114 (1996) 139–149.
[15] F.M. Mahfouz, Transient free convection from a horizontal cylinder placed in a micropolar fluid, Heat Mass Transfer 39 (2003) 455–462.
[16] T. Hsu, P. Hsu, S. Tsai, Natural convection of micropolar fluids in an enclosure with heat sources, Int. J. Heat Mass Transfer 40 (17) (1997) 4239–4249.
[17] S. Bhattacharyya, I. Pop, Free convection from cylinders of elliptic cross section in micropolar fluids, Int. J. Eng. Sci. 34 (1996) 1301–1310.
[18] W.M. Collins, S.C.R. Dennis, Flow past an impulsively started circular cylinder, J. Fluid Mech. 60 (1973) 105–127.
[19] H.M. Badr, S.C.R. Dennis, Time-dependent viscous flow past an impulsively started rotating and translating circular cylinder, J. Fluid Mech. 158 (1985) 447–488.
[20] F.M. Mahfouz, H.M. Badr, Flow structure in the wake of a rotationally oscillating cylinder, ASME J. Fluids Eng. 122 (2000) 290–301.
[21] T.H. Kuehn, R.J. Goldstein, Numerical solutions to the Navier-Stokes equations for laminar natural convection about a horizontal isothermal circular cylinder, Int. J. Heat Mass Transfer 23 (1980) 971–979.
[22] T. Saitoh, T. Sajik, K. Maruhara, Bench mark solutions to natural convection heat transfer problem around a horizontal circular cylinder, Int. J. Heat Mass Transfer 36 (5) (1993) 1251–1259.